J. Fluid Mech. (1986), *vol.* 164, *pp.* 337–358
Printed in Great Britain

Network models for two-phase flow in porous media Part 2. Motion of oil ganglia

By MADALENA M. DIAS
Schlumberger–Doll Research, Old Quarry Road, Ridgefield, CT06877, USA
AND ALKIVIADES C. PAYATAKES
Department of Chemical Engineering, University of Patras, *and* Research Institute of Chemical Engineering and High Temperature Chemical Processes, Patras 261 10, Greece

(Received 22 February 1985 and in revised form 30 July 1985)

The behaviour of non-wetting ganglia undergoing immiscible displacement in a porous medium is studied with the help of a theoretical simulator. The porous medium is represented by a network of randomly sized unit cells of the constricted-tube type. The fluid of a non-wetting ganglion is in contact with the wetting fluid at menisci which are assumed to be spherical cups. The flow in every constricted unit cell occupied by a single fluid is modelled as flow in a sinusoidal tube. The flow in every unit cell that contains a meniscus and portions of both fluids is treated with a combination of a Washburn-type analysis and a lubrication-theory approximation. The flow problem is thus reduced to a system of linear equations the solution of which gives the instantaneous pressures on the nodes, the flowrates through the unit cells, and the velocities of the menisci. The motion of a ganglion is determined by assuming quasi-static flow, taking a small time increment, updating the positions of the menisci, and iterating. The behaviour of solitary ganglia is studied under conditions of quasi-static displacement (*Ca* slightly larger than critical), as well as dynamic displacement (*Ca* substantially larger than critical). Shape evolution, rate of flow, mode of break-up, and stranding are examined. The stranding and break-up coefficients are determined as functions of the capillary number and the ganglion size for a 100×200 sandpack. The dependence of the average ganglion velocity on ganglion size, capillary number, viscosity ratio and dynamic contact angle is examined for the simple case of motion between straight rows of spheres. It is found, among other things, that when $\mu_o < \mu_w$ the velocity of ganglia can be substantially larger than that of the displacing fluid.

1. Introduction

Many important applications involve the displacement of a non-wetting fluid in a permeable medium by a wetting one. Gas and oil recovery from reservoir rock, irrigation, aquifer formation, imbibition during mercury porosimetry, are examples of such applications. In oil production the objective is to achieve high displacement efficiency by inexpensive means. The overall displacement efficiency is decided by the sweep efficiency and the microdisplacement efficiency. Here we are concerned with certain aspects of microdisplacement efficiency.

For the sake of brevity, in the rest of this article we will use the term oil instead of non-wetting fluid, and water instead of wetting fluid. This places emphasis on the

relevance of this work to oil recovery, but the results apply to any other pair of fluids with respectively similar properties.

When a porous medium filled with oil gets invaded by water, only a fraction of the oil gets displaced. The reason for this phenomenon is the following. As water invades the porous medium, it begins to form tortuous microfingers within the territory of the oil. The formation of these microfingers is due to the randomness of the pore structure, the interplay between viscous forces and capillary forces, the difference in viscosity between the two fluids, the formation of wetting films assisted by microroughness on the pore walls, etc. Before long, the growing microfingers begin to surround portions of the retreating oil and to disconnect them from the bulk of that phase. The disconnected segments of oil are called ganglia.

The formation of ganglia is a pivotal event. Before becoming disconnected, the oil in a ganglion-to-be was assisted in its motion by the capillary pressure. Once disconnection has occurred, the capillary pressure strongly opposes further motion of the ganglion. As a result, a ganglion gets stranded, at or near the position where it was formed. When the invasion of the water is complete, a large fraction of the original amount of oil remains entrapped in the form of ganglia. A review of works pertaining to microdisplacement and the formation of ganglia was given recently in Payatakes & Dias (1984). A new theoretical simulator of this process was developed in a companion publication (Dias & Payatakes 1986). Here, we will focus our attention on the behaviour of ganglia, when they get mobilized.

The mobilization of oil ganglia has been the object of several studies. Melrose & Brandner (1974) were the first to propose a mobilization criterion based on the competition between capillary pressure and external flow-field pressure. Batycky & Singhal (1977) made a careful analysis of the mobilization of a ganglion in a track between two rows of uniform spheres, and verified the basic concept behind the theory of entrapment and mobilization. Ng, Davies & Scriven (1978) made visualization experiments and reported agreement with the Melrose–Brandner criterion. A theoretical study of ganglion mobilization in a sinusoidal tube was made by Oh & Slattery (1979). Egbogah & Dawe (1981), Rapin (1980), Hinkley (1982), and Yadav & Mason (1983) reported experimental observations on ganglion motion and entrapment. Legait (1981) studied the motion of an oil droplet through a single constriction in a long tube, taking into account inertial, viscous and capillary forces. Legait & Jacquin (1982) studied the conditions under which an oil droplet passes through a square constriction in a long tube and they concluded that the critical Ca value depends on the geometry of the constriction and on the viscosity ratio. An experimental study of the motion of ganglia in sinusoidal tubes for Ca values of order 10^{-2} and higher was made by Olbricht & Leal (1983).

The behaviour of solitary ganglia and the collective behaviour of large populations of interacting ganglia are problems that arise in enhanced oil recovery (Payatakes, Ng & Flumerfelt 1980; Ng & Payatakes 1980; Payatakes 1982). They may also arise in cases when a porous medium filled with oil gets flooded from the beginning with water at high Ca value, say $Ca > 5 \times 10^{-4}$.

Based on experimental observations by Rapin (1980), Payatakes (1982) proposed that the motion of ganglia undergoing immiscible displacement can be classified either as quasi-static displacement, or as dynamic displacement. The distinction is based on the number of downstream menisci of the ganglion that are advancing at any given time. If the applied Ca value is slightly larger than the critical value required to mobilize the ganglion under consideration, the ganglion advances with only one of its downstream menisci at any instant, while one or more of its upstream menisci are also in motion. This type of behaviour is called quasi-static displacement. If, on

the other hand, the applied Ca value exceeds the critical one substantially, the ganglion advances with two or more of its downstream menisci simultaneously. This type of behaviour is called dynamic displacement. There are good reasons for making this distinction.

A ganglion undergoing quasi-static displacement has a tendency to get elongated, and to align itself with the macroscopic flow direction. However, owing to the randomness of the porous medium, it eventually breaks into two daughter ganglia (usually unequal), the smaller one of which, or both, may get stranded. Here, the mechanism of break-up is usually pinch-off. If a daughter ganglion does not get stranded immediately, it too undergoes quasistatic displacement. The mobilized ganglion may also get restranded without breaking up first, either because it meets a set of narrow throats, or because it gets stubby, or for both reasons.

A ganglion in dynamic displacement advances in two or more directions simultaneously, and as a result suffers frequent break-ups. This phenomenon is called dynamic break-up. In this way, the ganglion is reduced to many smaller ones, some of which may get stranded immediately, while others undergo dynamic displacement or quasi-static displacement. The frequency of dynamic break-up per unit length of migration is much higher than that of break-up during quasi-static displacement. Another, less important, difference is that the tendency of ganglia to become elongated and aligned with the macroscopic flow direction is not very pronounced during dynamic displacement.

A theoretical model of the behaviour of solitary ganglia in porous media was developed by Ng & Payatakes (1980) and Payatakes, Woodham & Ng (1981). That model predicts the 'steps' taken by a mobilized ganglion by applying at any given stage a ganglion-specific mobilization criterion. That criterion is a generalization of the Melrose–Brandner criterion and predicts not only whether another 'step' will be taken by the ganglion, but also the next position of the ganglion in the network, and whether break-up will occur during this step or not. The Ng & Payatakes model explains the phenomena of ganglion elongation and alignment with the flow, and also predicts the coefficients of stranding and break-up. Its major shortcomings are that it applies only to quasi-static displacement and that it has nothing to say about rates and the ganglion velocity. It must be noted here that the average ganglion velocity is a key parameter in the dynamics of oil-ganglion populations.

In the present work we present a flow simulator that applies to both quasi-static and dynamic displacement, predicts pressure fields and flowrates, and gives the velocity of ganglia as a function of geometrical and physical parameters.

2. Model formulation: boundary conditions

The simulator used here is the same as that described in Part 1 of this paper (Dias & Payatakes 1986). Here we discuss some details of the boundary conditions that are of special interest to oil-ganglion flow.

The absolute permeability, k, of a specified network of randomly sized unit cells can be calculated independently, by imposing a constant macroscopic pressure gradient and averaging the calculated permeability values obtained from a number of realizations (Ng 1980; Dias & Payatakes 1986).

For a specified value of Ca the magnitude of the corresponding macroscopic pressure gradient in a network with one ganglion (or in a very sparsely populated network) is given by

$$-\nabla P = \frac{\sigma_{ow} Ca}{k}, \tag{1}$$

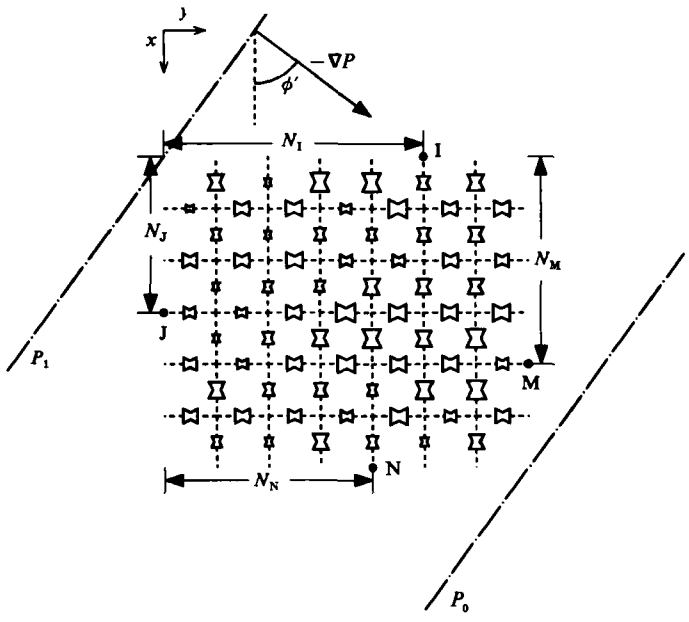

FIGURE 1. Example of flow configuration. The direction of the macroscopic pressure gradient $(-\nabla P)$ forms an angle ϕ' with the z-axis.

where σ_{ow} is the oil–water interfacial tension. This approximation is valid so long as the oil ganglion is small when compared with the network size so that the network itself can be considered as virtually oil-free and the presence of the oil ganglion is not discernible at the network boundaries.

In setting up the simulation we must specify the size of the network (N_x and N_y) and the macroscopic-pressure-gradient direction. The direction of the macroscopic pressure gradient is given by ϕ', which is defined as the angle between the x-axis and the direction of the macroscopic pressure gradient. Let us consider two planes normal to the macroscopic-pressure-gradient direction (figure 1). The pressure drop along the network is then given by

$$P_1 - P_0 = (-\nabla P)\, l D_{xy}, \tag{2}$$

where

$$D_{xy} = N_y \sin\phi' + N_x \cos\phi', \tag{3}$$

and P_1 and P_0 represent the pressures at planes 1 and 0, respectively. For simplicity, P_0 is given the value zero. The pressures at each boundary node can easily be derived using geometrical considerations. For example, the pressures at locations I, J, M and N in figure 1 are given respectively by

$$P_I = (-\nabla P)\, l(D_{xy} - N_I \sin\phi'), \tag{4a}$$

$$P_J = (-\nabla P)\, l(D_{xy} - N_J \cos\phi'), \tag{4b}$$

$$P_M = (-\nabla P)\, l(D_{xy} - N_y \sin\phi' - N_M \cos\phi'), \tag{4c}$$

$$P_N = (-\nabla P)\, l(D_{xy} - N_z \cos\phi' - N_N \sin\phi'), \tag{4d}$$

where N_I and N_N are the number of branches along the y-axis up to the locations I and N, respectively, and N_J and N_M are the number of branches along the x-axis up to the locations J and M, respectively.

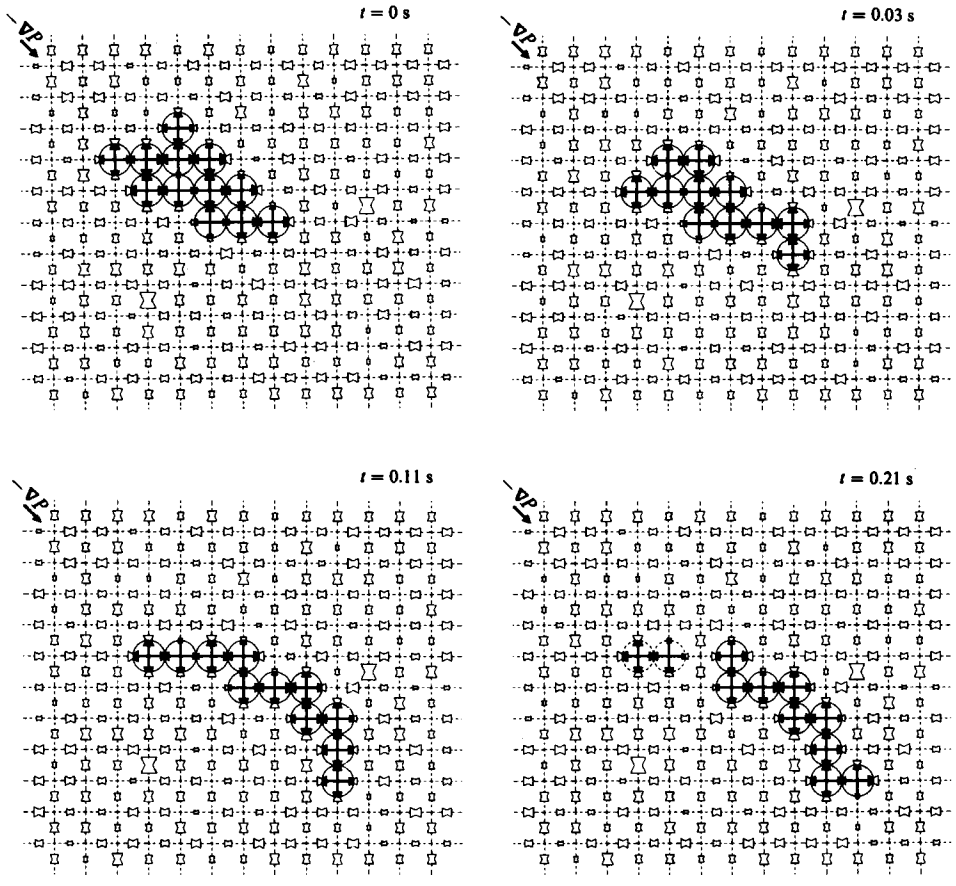

FIGURE 2. Stages of the simulated motion of a 12-CEVS ganglion in a network representing a 100×200 sandpack for $Ca = 2 \times 10^{-4}$, $\kappa = 1$, and $\phi' = 45°$.

3. Sample stochastic simulations of ganglion fate: quasi-static and dynamic displacements

All the simulations in this work were done on a network representing a 100×200 sandpack having a porosity of 0.395 and grain sizes ranging from 74 to 149 μm. The throat size distribution and other pertinent parameters of the porous-medium model were obtained by Payatakes *et al.* (1980), using the method developed in Payatakes, Tien & Turian (1973) and the data reported by Leverett (1941). The experimental permeability of this sandpack is $k = 3.55 \times 10^{-8}$ cm^2, and the calculated permeability for the two-dimensional network is $k = 2.78 \times 10^{-8}$ cm^2.

The fate of a solitary oil ganglion depends on various physical operational parameters, among which the most important are the capillary number, the direction of the macroscopic pressure gradient, the size, shape and orientation of the ganglion, and the local geometry of the porous medium. The influence of each of these factors has been illustrated by Dias (1984). Here we report simulations showing the effects of the capillary number and of the direction of the macroscopic pressure gradient relative to the axes of the network.

Consider the simulations shown in figures 2, 3, and 4. In order to isolate the effect of the capillary number, all three simulations were performed on the same random network, with a viscosity ratio of unity ($\kappa = 1$), perfect wetting conditions

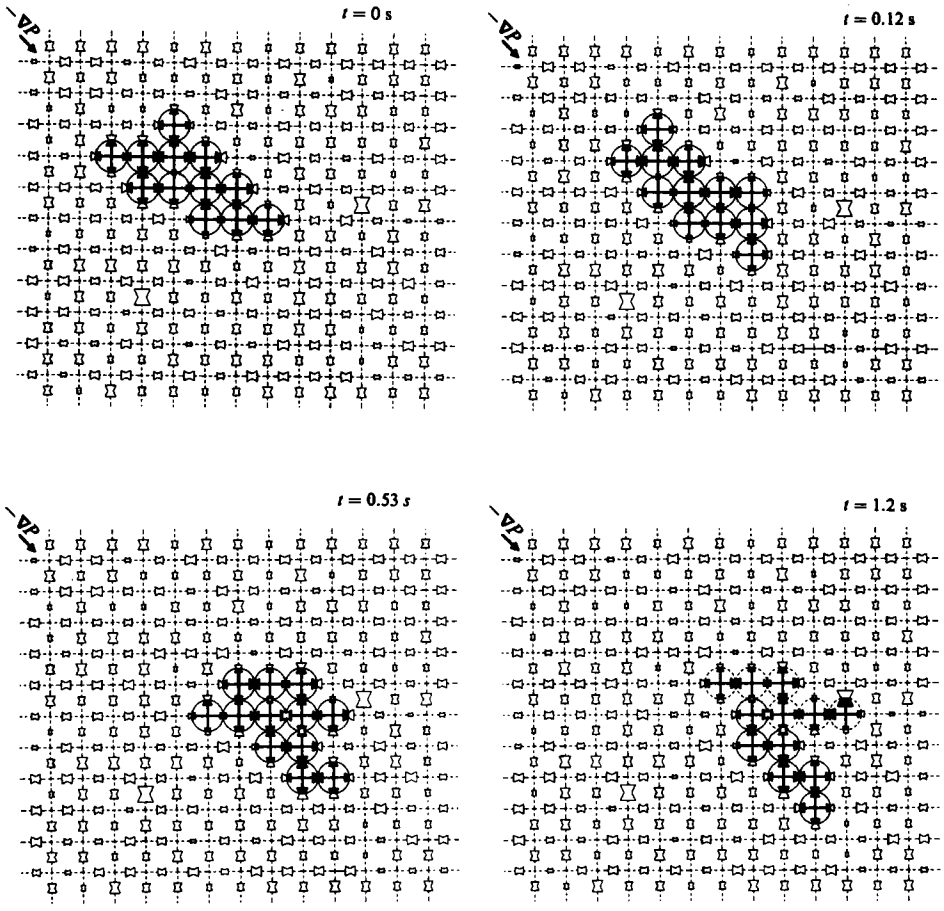

FIGURE 3. Stages of the simulated motion of as 12-CEVS ganglion in a network representing a 100×200 sandpack for $Ca = 4 \times 10^{-4}$, $\kappa = 1$, and $\phi' = 45°$.

($\theta_e = \theta_a^o = \theta_r^o = 0°$), and the direction of the macroscopic pressure gradient set at 45°.

In figure 2 the capillary number is set at a value just capable of inducing motion ($Ca \approx Ca_{cr}$, where Ca_{cr} is the critical capillary number for mobilization of the ganglion under consideration). As expected, the ganglion begins to advance with one downstream meniscus at a time. The motion is somewhat episodic, in the sense that it is characterized by a relatively large period during which the downstream interface creeps through a constriction, and a relatively short period during which oil invades the downstream chamber – once the interface passes through the constriction. The occurrence of a xeron (invasion by oil of a downstream chamber) is always accompanied by the occurrence of a hygron (invasion of an upstream chamber by water). As the ganglion moves forward it elongates and aligns itself with the direction of the macroscopic pressure gradient. At some stage of the simulation, an oil thread is formed and the ganglion breaks into two daughter ganglia. The smaller ganglion gets stranded while the larger one continues to move forward. These observations are in close agreement with the characteristics of the quasi-static displacement of ganglia described by Payatakes (1982). The mode of break-up observed in this simulation, resulting solely from the rupture of an oil thread (pinch-off), is very

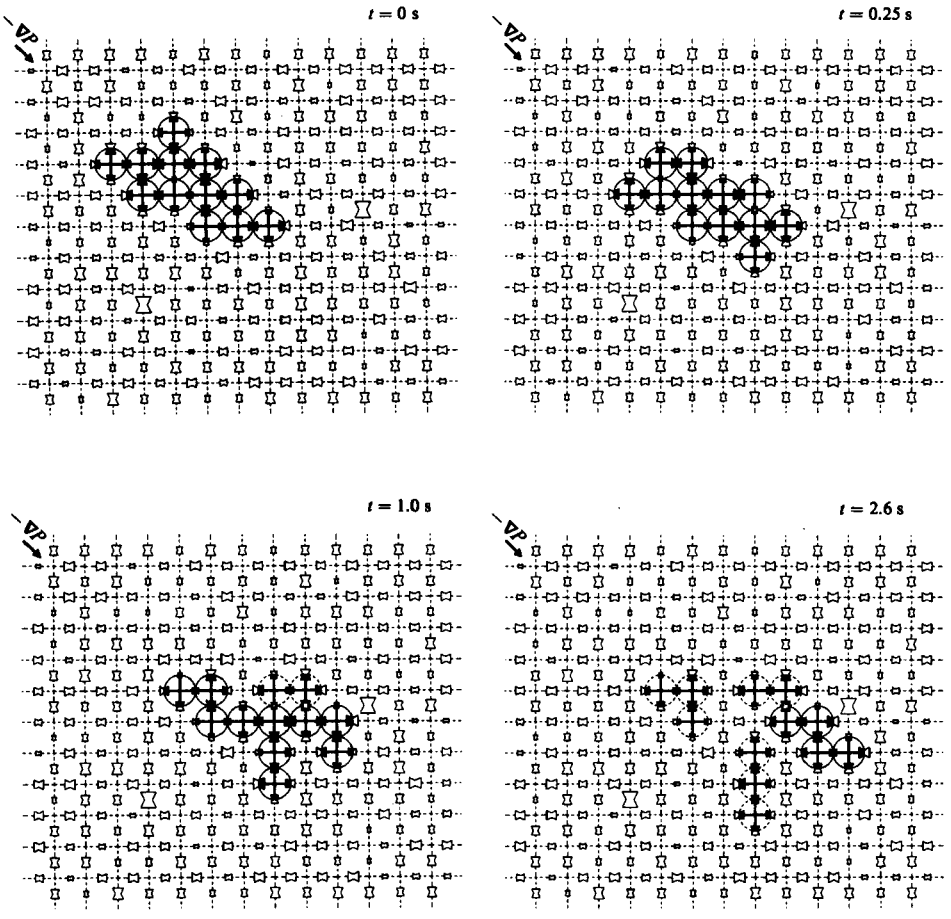

FIGURE 4. Stages of the simulated motion of as 12-CEVS ganglion in a network representing a 100×200 sandpack for $Ca = 10^{-3}$, $\kappa = 1$, and $\phi' = 45°$.

common in quasi-static displacement, and it usually results in two differently sized daughter ganglia.

Figure 3 and 4 show the same ganglion subject now to larger values of Ca. In the simulation shown in figure 3, the capillary number is set at a value roughly twice the critical value for mobilization. The ganglion now advances with two menisci simultaneously, thus forming two branches. This type of microdisplacement is called dynamic displacement. As the displacement proceeds the ganglion eventually breaks into two similarly sized daughter ganglia. This mode of break-up, resulting from the simultaneous advance of two or more menisci, is an inevitable consequence of dynamic displacement and it is called dynamic break-up (Payatakes 1982; Payatakes & Dias 1984). An interesting observation on this particular simulation is that, although the original ganglion suffers dynamic break-up, the two resulting daughter ganglia have elongated forms and move with quasi-static displacement without breaking for several subsequent steps. The explanation for this behaviour is that, although the capillary number is sufficiently large to induce dynamic displacement of the large original ganglion, it is only large enough to induce quasi-static displacement of the smaller daughter ganglia.

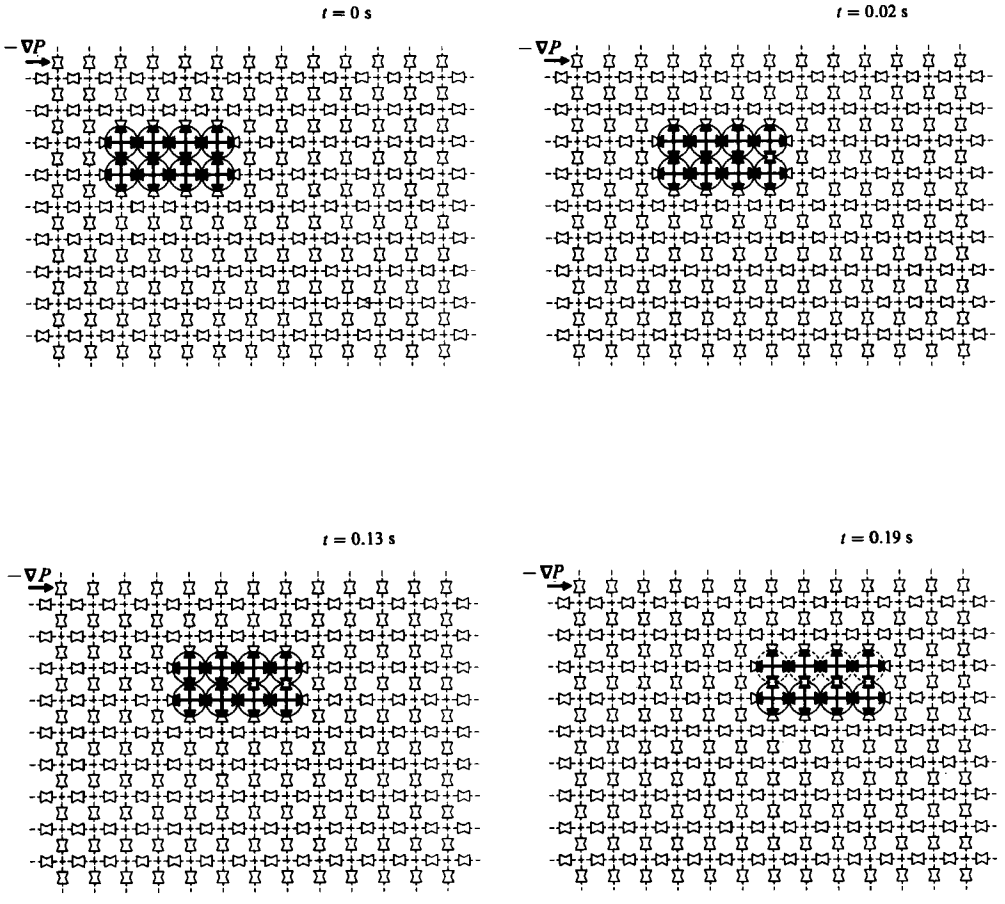

FIGURE 5. Stages of the simulated motion of a 8-CEVS ganglion in a network of monosized unit cells for $Ca = 10^{-3}$, $\kappa = 7$, and $\phi' = 90°$.

In the last case (figure 4), Ca is set at a value much higher than Ca_{cr}.The ganglion now advances with several menisci simultaneously and breaks into several daughter ganglia, some of which get stranded, while the others continue to move on, and, in turn, break into other ganglia. Thus, the original ganglion rapidly disintegrates into many small ones. It should be noted that, although most of this disintegration is due to dynamic break-up, some cases of pinch-off are also observed.

An important finding is that, whereas the network is macroscopically isotropic for one-phase flow (Dias 1984), it is anisotropic for two-phase flow. Figures 5, 6 and 7 demonstrate the effects of changing the direction of the macroscopic pressure gradient. A network of monosized unit cells is used in all three figures in order to remove the effect of randomness from the results. The capillary number is set at $Ca = 10^{-3}$, and the viscosity ratio at $\kappa = 7$.

In figure 5 the macroscopic pressure gradient is aligned with the longitudinal axis of the network, $\phi' = 90°$. Both frontal interfaces advance simultaneously and the ganglion develops two prongs. Coalescence of the two prongs is not allowed (it would not occur anyway due to the lack of a lateral pressure difference), so the ganglion eventually splits into two similar ganglia.

When $\phi' = 70°$ (figure 6), the ganglion tends to elongate in the direction of the

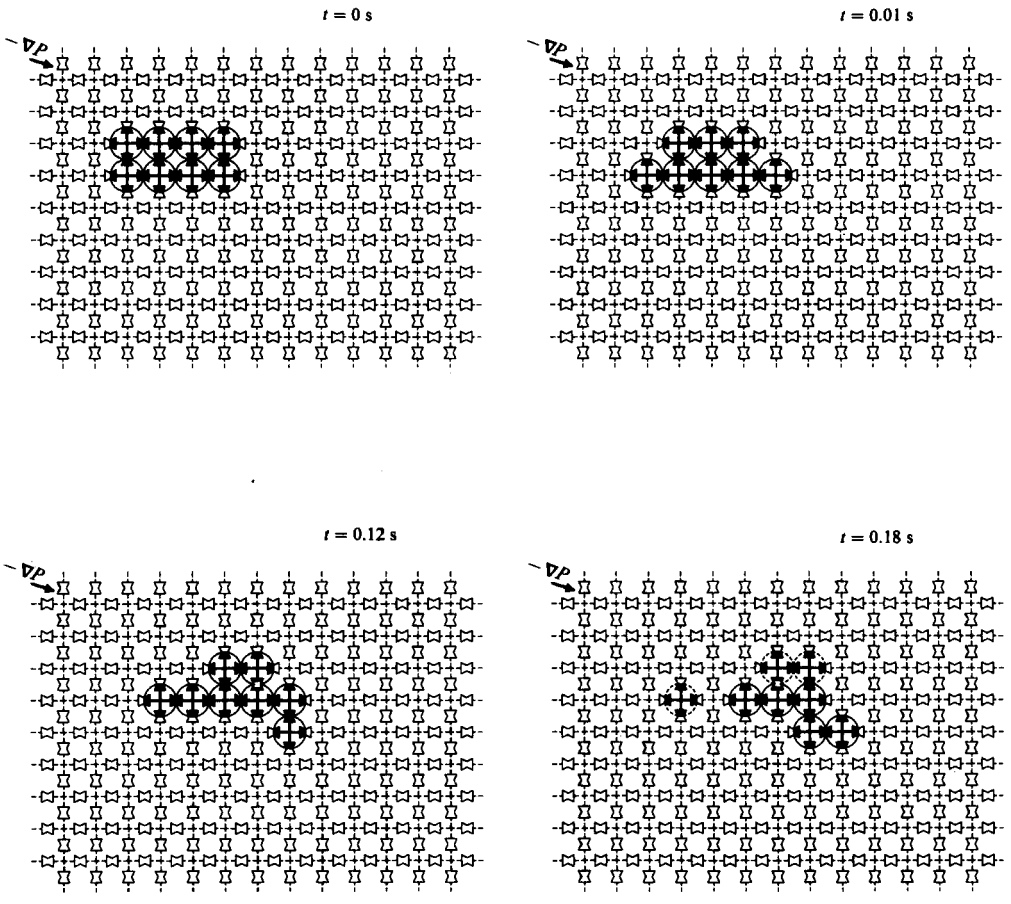

FIGURE 6. Stages of the simulated motion of a 8-CEVS ganglion in a network of monosized unit cells for $Ca = 10^{-3}$, $\kappa = 7$, and $\phi' = 70°$.

macroscopic pressure gradient; however, as it moves it finds itself in situations that cause pinch-off and dynamic break-up simultaneously.

Finally, in figure 7, the direction of the macroscopic pressure gradient is set at $\phi' = 45°$. The ganglion advances with two menisci simultaneously, and breaks into two daughter ganglia, which, in turn break again through dynamic break-up, and the resulting four ganglia get stranded.

The implications of these observations for the design of experiments and the interpretation of the results thereof are clear.

4. Stranding and break-up

4.1. *The stranding and the break-up coefficients*

Payatakes *et al.* (1980) expressed the effects of stranding and break-up on oil-ganglion dynamics in terms of the stranding coefficient, λ, and the break-up coefficient, ϕ. The dependence of these coefficients on ganglion size and the capillary number was studied in Ng & Payatakes (1980) for the case of quasi-static displacement. Here we will make a more detailed and general study.

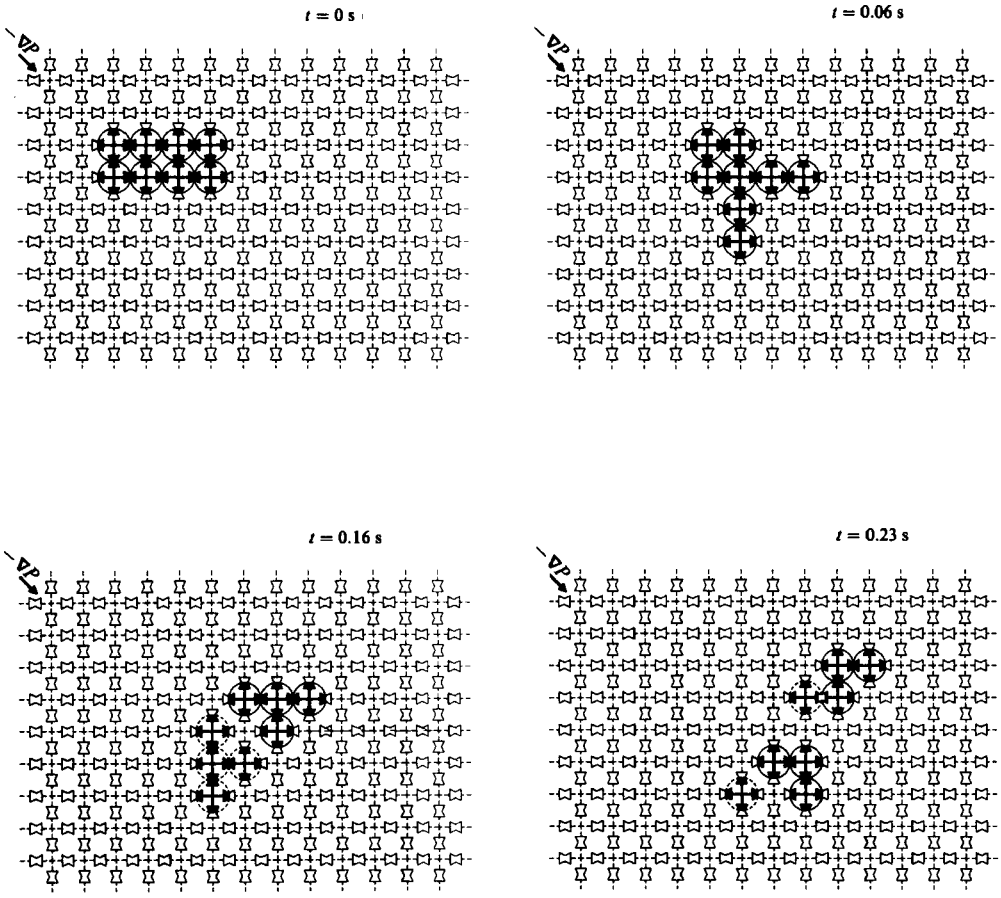

FIGURE 7. Stages of the simulated motion of a 8-CEVS ganglion in a network of monosized unit cells for $Ca = 10^{-3}$, $\kappa = 7$, and $\phi' = 45°$.

Clearly, the fate of a single ganglion depends not only on the size of the ganglion but also on its shape and orientation. However, the task of characterizing each ganglion by all these variables seems difficult, and time consuming. Following Payatakes *et al.* (1980) we characterize a ganglion only by its volume. A v-ganglion is defined as one having volume between v and $v+\Delta v$. The reduced ganglion volume is defined as $v^* = v/v_{\mathrm{CEVS}}$ and v_{CEVS} is the mean volume of the conceptual elemental void space.

Consider an initial population of v-ganglia distributed between two planes which are normal to the main flow direction and are separated by a small distance δ. At time $t = 0$ an immiscible flood starts flowing past the oil ganglia. Neglecting axial dispersion and assuming that the ganglion population is sufficiently sparse that collisions between ganglia are unlikely, this 'plug' of v-ganglia will begin to migrate downstream with velocity $\bar{u}_z(v; \boldsymbol{a}_1)$, where $\boldsymbol{a}_1$ is a parameter vector (with elements Ca, κ, θ, etc.). As the v-ganglia move, their concentration is reduced due to stranding and break-up.

Let $n(z, t; v)\,\Delta v$ be the number of moving v-ganglia per unit porous-medium volume at position z and time t. Ng & Payatakes (1980) showed that, if λ and ϕ are constant, then $n(z, t; v)$, as seen by an observer travelling with the plug, is given by

$$n(z, \tau; v) = n_0 \exp\left[-(\lambda+\phi)\, z\right], \tag{5}$$

where n_0 is the initial value of $n(t, z; v)$, τ is the corrected time defined as

$$\tau = t - \frac{z}{\bar{u}_z(v; \boldsymbol{a}_1)}, \tag{6}$$

and the stranding and the break-up coefficients, λ and ϕ, are defined as

$$\lambda = -\frac{1}{n}\frac{\partial n}{\partial z}\bigg|_{\text{due to stranding}}, \tag{7}$$

$$\phi = -\frac{1}{n}\frac{\partial n}{\partial z}\bigg|_{\text{due to break-up}}. \tag{8}$$

The number of stranded v-ganglia per unit porous-medium volume at position z and time τ, $\sigma(z, \tau; v)\,\Delta v$, and the number of v-ganglia that fissioned per unit porous-medium volume at position z and time τ, $\beta(z, \tau; v)\,\Delta v$, are given by

$$\sigma(z, \tau; v) = \lambda \delta n_0 \exp\left[-(\lambda+\phi)\,z\right], \tag{9}$$

$$\beta(z, \tau; v) = \phi \delta n_0 \exp\left[-(\lambda+\phi)\,z\right], \tag{10}$$

assuming again that λ and ϕ are constant.

Plotting $\ln(n/n_0)$ versus z/l, a straight line with intercept unity and slope $-(\lambda+\phi)\,l$ is obtained. Similarly, plots of $\ln(\sigma\lambda/\delta n_0)$ and $\ln(\beta l/\delta n_0)$ versus z/l give straight lines with slope $-(\lambda+\phi)\,l$ and intercepts $\ln(\lambda l)$ and $\ln(\phi l)$, respectively. This linearity is a consequence of the assumption that λ and ϕ are not functions of z and have values which are averages over the ensemble of all possible shapes. However, if a ganglion elongates as it moves (see figure 2), its probabilities of break-up and stranding are reduced, and λ and ϕ may very well be functions of z. In such cases the three curves $\ln(n/n_0)$ versus z/l, $\ln(\sigma l/\delta n_0)$ versus z/l, and $\ln(\beta l/\delta n_0)$ versus z/l deviate from linearity. This effect was first investigated by Payatakes *et al.* (1981). That work, however, was based on repeated application of the mobilization criterion mentioned earlier. Here we make a more detailed analysis based on the network solution of the flow problem.

For a fixed ganglion volume and random initial shapes, many simulations are undertaken with the same Ca and κ values, in each simulation allowing the ganglion to migrate until it either breaks or gets stranded. Superimposing the starting planes of all simulations and considering the entire ensemble of results, values of (n/n_0), $(\sigma l/\delta n_0)$, and $(\beta l/\delta n_0)$ can be determined. To this end, we consider several positions along z, and we count the number of moving v-ganglia at each position z, the number of stranded v-ganglia left in the interval $(z-\frac{1}{2}\Delta z, z+\frac{1}{2}\Delta z)$, and the number of fissions of v-ganglia in the same interval. The following variables are readily obtained:

$$\chi = \frac{\text{number of } v\text{-ganglia moving at position } z}{\text{initial number of } v\text{-ganglia}}, \tag{11}$$

$$\psi = \frac{\text{number of } v\text{-ganglia stranded in the interval } (z \pm \frac{1}{2}\Delta z)}{\text{initial number of } v\text{-ganglia}}, \tag{12}$$

$$\omega = \frac{\text{number of } v\text{-ganglia fissioned in the interval } (z \pm \frac{1}{2}\Delta z)}{\text{initial number of } v\text{-ganglia}}. \tag{13}$$

Provided that Δz is sufficiently small, say $(\Delta z \ll l)$, the values of χ, $(\psi l/\Delta z)$, and $(\omega l/\Delta z)$, can be regarded as the local 'experimental' values of (n/n_0), $(\sigma l/\delta n_0)$, and $(\beta l/\delta n_0)$, respectively. Plotting the logarithms of $(\psi l/\Delta z)$ and $(\omega l/\Delta z)$ versus z/l, the values of λl and ϕl may be obtained by simple fitting.

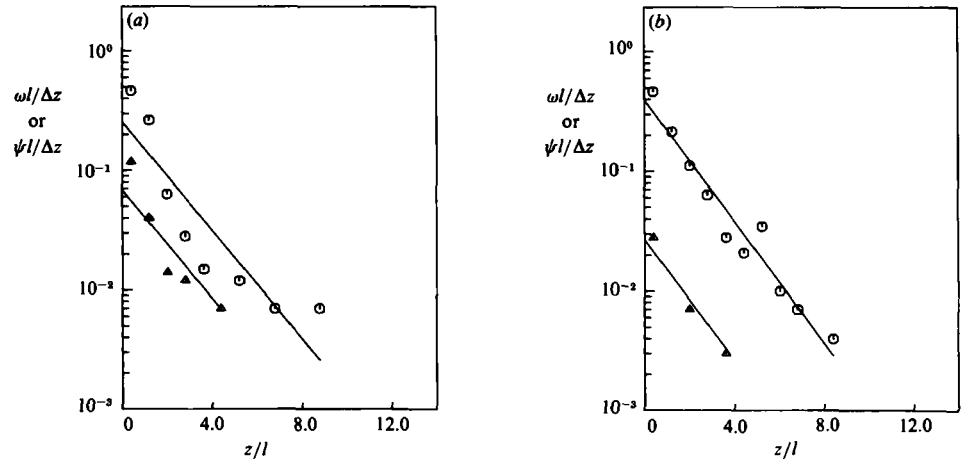

FIGURE 8. Plots of $(\omega l/\Delta z)$ and $(\psi l/\Delta z)$, *vs.* the normalized length of migration, z/l, in a 100×200 sandpack, for a 5-CEVS ganglion, $\kappa = 7$ and (*a*) $Ca = 10^{-3}$; (*b*) $Ca = 5 \times 10^{-3}$.

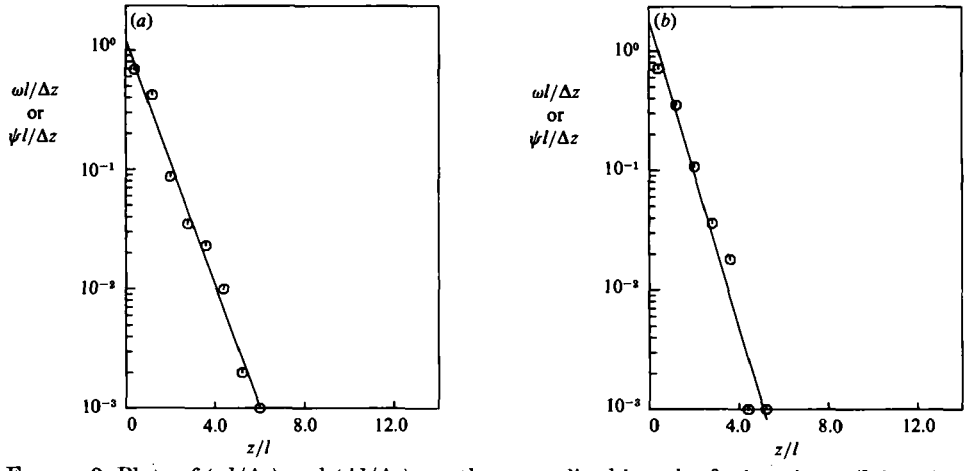

FIGURE 9. Plots of $(\omega l/\Delta z)$ and $(\psi l/\Delta z)$, *vs.* the normalized length of migration, z/l, in a 100×200 sandpack, for a 210-CEVS ganglion, $\kappa = 0.6$ and (*a*) $Ca = 10^{-3}$; (*b*) $Ca = 5 \times 10^{-3}$.

Typical results of this study for 5-CEVS and 15-CEVS ganglia are shown in figures 8 and 9. In each case the initial shape of the ganglion is chosen randomly from among all possible shapes. In figure 9 the plot $(\psi l/\Delta z)$ versus z/l is omitted, since too few ganglia were stranded to obtain statistically meaningful values. Inspection of these results leads to the following observations:

- Stranding of ganglia decreases as the capillary number and the ganglion size increase. For fixed Ca, λl becomes nil for sufficiently large ganglia.
- High capillary numbers and large ganglion sizes increase the rate of ganglion break-up.
- For small values of Ca and medium-sized ganglia ($v^* = 4$–7), the curves show a significant deviation from linearity, implying the presence of elongation effects.
- As the viscosity ratio, κ, increases, the rate of stranding increases, whereas the rate of break-up decreases. The increase in the rate of stranding is stronger than the decrease of break-up.

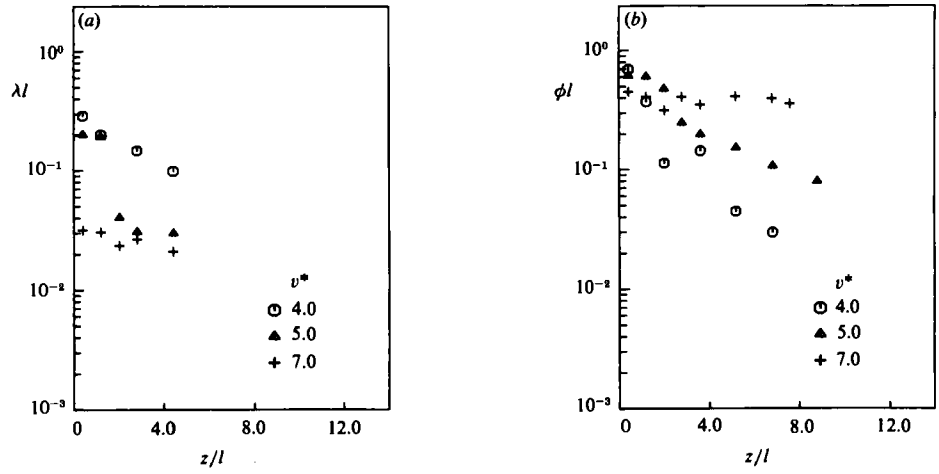

FIGURE 10. Plots of the dimensionless stranding coefficient, λl, and of the dimensionless break-up coefficient, ϕl, *vs.* the normalized length of migration, z/l, in a 100×200 sandpack, for 4, 5 and 7-CEVS ganglia, $\kappa = 7$ and $Ca = 10^{-3}$.

The first three observations are in accordance with previous observations (Ng & Payatakes 1980; Rapin 1980; Payatakes *et al.* 1981) and with the ganglia velocity results reported in the previous section. The fourth observation is a new result.

In order to investigate the effects of elongation, the local values of λl and ϕl are calculated at each position z/l. From simple v-ganglion balances we obtain

$$\sigma = -\delta \left[\frac{\partial n(z, \tau; v)}{\partial z}\right]_{\text{due only to stranding}}, \tag{14}$$

$$\beta = -\delta \left[\frac{\partial n(z, \tau; v)}{\partial z}\right]_{\text{due only to breakup}}. \tag{15}$$

Combining (7) and (14), and (8) and (15), we get

$$\lambda = \frac{1}{\delta} \frac{\sigma(z, \tau; v)}{n(z, \tau; z)}, \tag{16}$$

$$\phi = \frac{1}{\delta} \frac{\sigma(z, \tau; v)}{n(z, \tau; z)}. \tag{17}$$

Recalling that the 'experimental' value of (n/n_0), $(\sigma l \delta n_0)$, and $(\beta l/\delta n_0)$, are given by χ, $(\psi l/\Delta z)$, and $(\omega l/\Delta z)$, respectively, the values of λl and ϕl at various positions can be calculated from

$$\lambda l = \frac{\psi l/\Delta z}{\chi} \quad \text{at fixed } z/l, \tag{18}$$

$$\phi l = \frac{\omega l/\Delta z}{\chi} \quad \text{at fixed } z/l. \tag{19}$$

Values of λl and ϕl versus z/l for 4-CEVS, 5-CEVS and 7-CEVS ganglia are plotted in figure 10 for $Ca = 10^{-3}$ and $\kappa = 7$. These plots confirm that there exists a dependency of both λl and ϕl on length of travel, especially for small ganglia. These findings are in accordance with the results reported by Payatakes *et al.* (1981), except that, in their work, the dependence of ϕl on zl was not so strong and presented a more erratic behaviour.

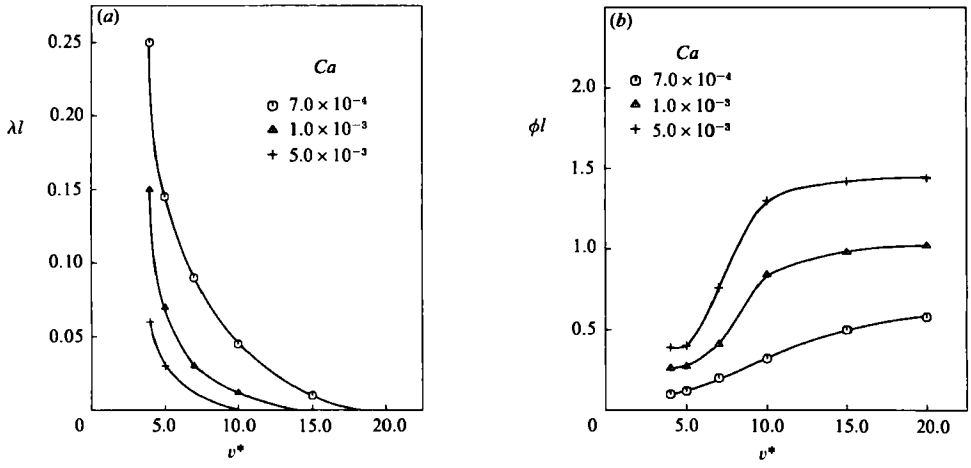

FIGURE 11. Plots of (*a*) the dimensionless stranding coefficient, λl, and (*b*) the dimensionless break-up coefficient, ϕl, *vs.* the reduced ganglion volume, v^*, in a 100×200 sandpack, for $\kappa = 7$ and various Ca values.

In order to summarize and compare these results, the break-up coefficient and the stranding coefficient are plotted versus ganglion size for various capillary numbers in figure 11. The plot of λl is given only for the case of $\kappa = 7$ due to the scarcity of data points in other cases. In general, an increase of the capillary number results in an increase of the break-up coefficient, probably due to the increase of dynamic break-up. The role of the viscosity ratio in the break-up coefficient is not very clear or very strong. It seems from these simulations that, once a ganglion is mobilized, its chances of breaking are nearly the same, independently of its viscosity. However, this may be an artifact, due to the fact that our criterion for break-up is based on a quasi-static analysis which by definition ignores the role of viscosity. Future work should try to make improvements in this area.

Finally, the probability of break-up increases significantly with ganglion size, whereas the probability of stranding decreases. As a general observation, solitary or non-interacting ganglia moving in random porous media are destined to split into smaller and smaller daughter ganglia, which in turn have a high probability of getting stranded. This observation is in agreement with the conclusions of Payatakes *et al.* (1980) and Ng & Payatakes (1980).

4.2. *Mode of break-up*

An important parameter in the dynamics of oil-ganglion populations is the break-up mode probability, $W(w, v)\,\Delta v$, defined as the probability that a moving w-ganglion will break into two daughter ganglia, one of which is a v-ganglion. The effect of the capillary number on $W(w, v)\,\Delta v$ is shown in figure 12. The viscosity ratio does not seem to affect the outcome of this function in any systematic or appreciable way. We make the following observations:

- For given v^*, $W(w, v)\,\Delta v$ increases as the size of the mother ganglion w decreases. This means that small daughter ganglia are more likely to be produced from the break-up of small mother ganglia.
- For low capillary numbers $W(w, v)\,\Delta v$ decreases monotonically with v^*. This means that pinch-off (which predominates for small Ca values) usually produces one small daughter ganglion and one larger ganglion.

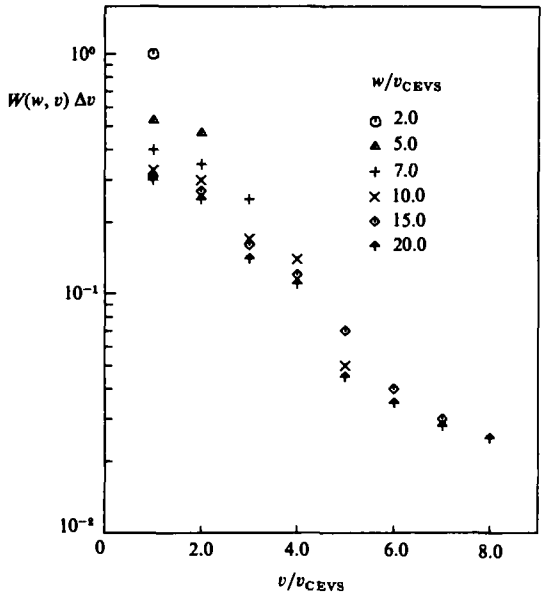

FIGURE 12. Plot of the break-up mode probability, $W(w, v)\,\Delta v$, *vs.* the reduced ganglion volume, v^*, in a 100×200 sandpack, for $\kappa = 7$ and $Ca = 10^{-3}$, with the mother ganglion reduced ganglion volume, w/v_{CEVS}, as a parameter. The right half of the plot is not shown since it is symmetrical.

- The probability that a large ganglion will generate a 1 or 2 CEVS daughter ganglion decreases slightly as the capillary number increases, whereas the probability that the break-up will give daughter ganglia of comparable sizes increases. This is due to the fact that dynamic break-up (which predominates at large Ca values) usually produces two daughter ganglia of comparable sizes.
- $W(w, v)\,\Delta v$ approaches a relatively small asymptotic value for very large ganglia ($v^* \geqslant 15$).

5. Ganglion velocity

One of the most important parameters in ganglion dynamics is the ganglion velocity, u_z (Payatakes 1980). Owing to the converging–diverging character and the randomness of the porous medium, the velocity of a ganglion varies with time, even if the flooding conditions are kept constant. Hence the ganglion velocity is expressed in terms of the time-averaged velocity with which the centroid of the ganglion migrates downstream, $\bar{u}_z$.

In the previous section we saw that ganglia moving in random porous media split into smaller daughter ganglia frequently. In order to avoid the problem of frequent break-up, Hinkley (1982) measured the velocity of ganglia experimentally by placing them in rectilinear tracks (formed by packing uniform glass beads), and by applying a macroscopic pressure gradient parallel to the tracks. The velocity of a ganglion was calculated by dividing the distance travelled by the centroid of the ganglion by the time elapsed. Ganglia tend to elongate until a cruising shape is attained. To ensure that this elongation effect did not affect the velocity calculations, each ganglion was allowed to travel a distance equal to twice its length, before the measurement began. From this point on, the ganglion velocity was calculated after the occurrence of each

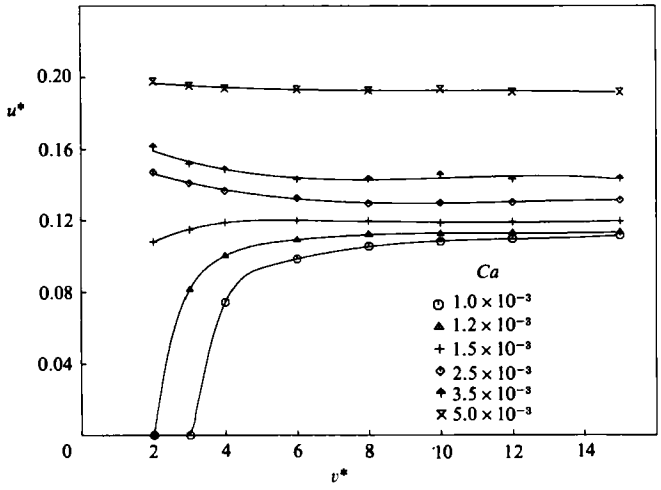

FIGURE 13. Plot of the reduced time-averaged ganglion velocity, u^*, *vs.* the reduced ganglion volume, v^*, in a 100×200 sandpack for various Ca values. $\kappa = 7$, $\theta_e = \theta_a^o = \theta_r^o = 0°$.

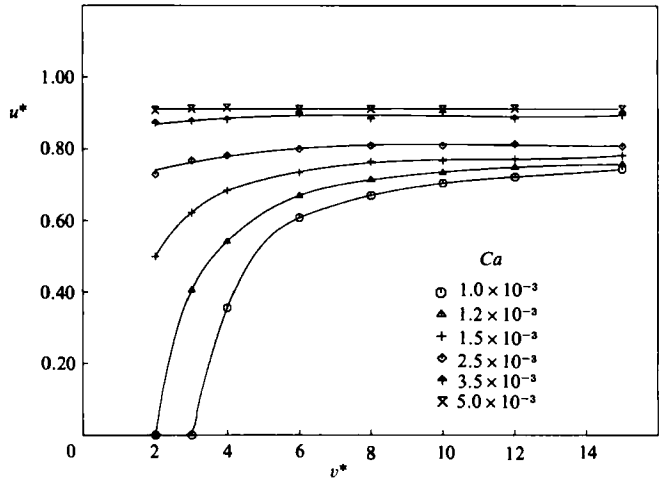

FIGURE 14. Plot of the reduced time-averaged ganglion velocity, u^*, *vs.* the reduced ganglion volume, v^*, in a 100×200 sandpack for various Ca values. $\kappa = 1$, $\theta_e = \theta_a^o = \theta_r^o = 0°$.

rheon, and its final value was recorded when the last three measurements converged to the same average value. In the present work we perform a set of theoretical calculations under similar conditions.

In order to make a first check of the validity of the calculations, a ganglion with the same viscosity as that of the water and with a null ganglion–water interfacial tension was placed in the network. This is equivalent to tracking a ganglion of coloured water being displaced by water. As expected, the average velocity of this ganglion was found to be the same as the mean interstitial velocity of the wetting phase in a network free of the non-wetting phase, V_i, which can be expressed as $V_i = V_f/\epsilon$. Here, V_f is the superficial velocity of the flood, and ϵ is the porosity of the porous medium. With this result in mind, the reduced time-averaged ganglion velocity is defined as $u^* = \bar{u}_z/V_i$. Under creeping-flow conditions, u^* is a function of Ca, v^*, θ, and the geometric parameters defining the porous-medium structure.

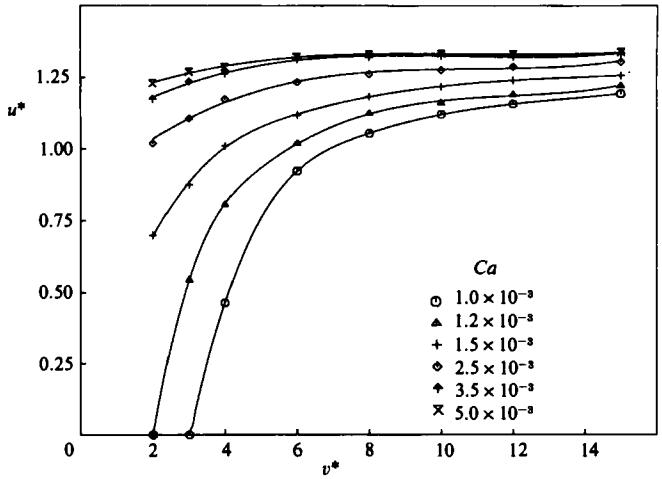

FIGURE 15. Plot of the reduced time-averaged ganglion velocity, u^*, *vs.* the reduced ganglion volume, v^*, in a 100×200 sandpack for various Ca values. $\kappa = 0.6$, $\theta_e = \theta_a^o = \theta_r^o = 0°$.

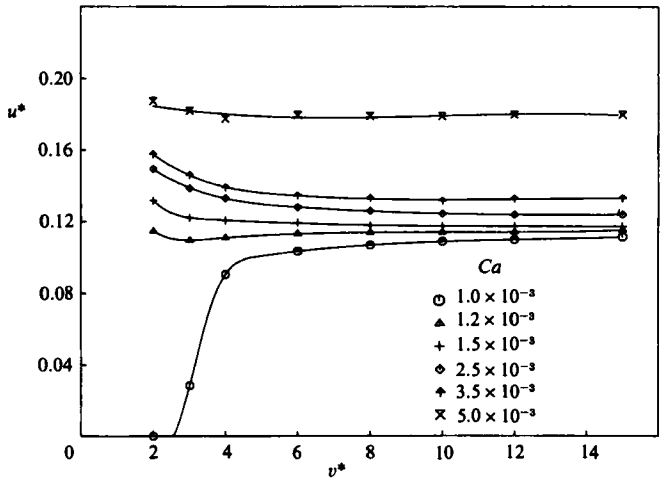

FIGURE 16. Plot of the reduced time-averaged ganglion velocity, u^*, *vs.* the reduced ganglion volume, v^*, in a 100×200 sandpack for various Ca values, $\kappa = 7$, $\theta_e = \theta_a^o = \theta_r^o = 10°$.

The simulator developed in this work applies to ganglia with sizes larger than, say, 2 to 3 CEVS, due to the Washburn-type approximation it adopts. The validity of the model was tested by comparing Hinkley's experimental velocities against the predicted theoretical velocities. To this end we determined the network parameters that pertain to Hinkley's porous medium, and calculated the ganglion velocities by applying the network simulator. We found good agreement between experimental and theoretical results (Dias 1984; Hinkley, Dias & Payatakes 1986).

After these tests, we calculated values of u^* in a 100×200 sandpack for various sets of parameter values, figures 13 to 18. These figures show how the ganglion size, the capillary number, the viscosity ratio, the equilibrium contact angle, and the existence (or absence) of contact-angle hysteresis and the rate-dependency of contact angles affect the velocity of ganglia in rectilinear tracks.

The influences of Ca, κ and v^* are shown in figures 13 to 15, for the case of perfect wetting conditions, namely $\theta_e = \theta_a^o = \theta_r^o = 0°$. We make the following observations:

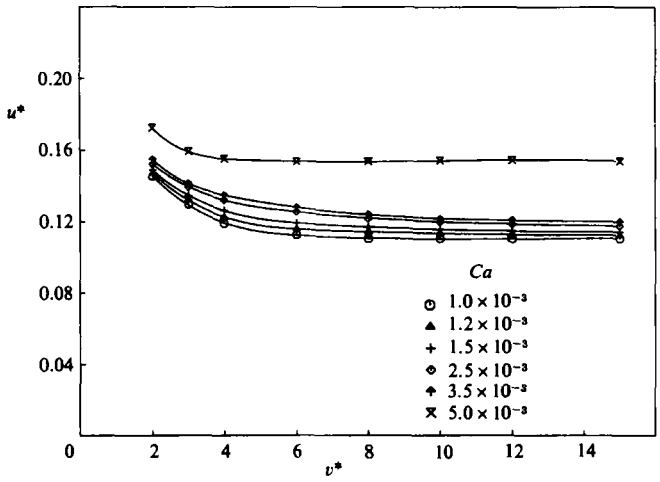

FIGURE 17. Plot of the reduced time-averaged ganglion velocity, u^*, *vs.* the reduced ganglion volume, v^*, in a 100×200 sandpack for various Ca values, $\kappa = 7$, $\theta_e = \theta_a^o = \theta_r^o = 30°$.

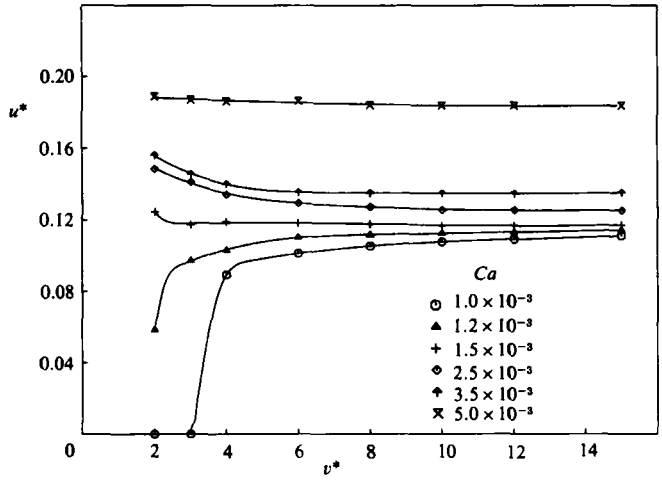

FIGURE 18. Plot of the reduced time-averaged ganglion velocity, u^*, *vs.* the reduced ganglion volume, v^*, in a 100×200 sandpack for various Ca values, $\kappa = 7$, $\theta_e = 10°$, $\theta_a^o = 11.4°$, $\theta_r^o = 0°$. The rate-dependency of the contact angle is shown in the insert.

- For $\kappa > 1$, the reduced time-averaged ganglion velocity is smaller than unity. This means that the average velocity of the oil is smaller than the average velocity of the water.
- For $\kappa < 1$ the reduced time-averaged ganglion velocity can be larger than unity. This means that the average velocity of the oil can be larger than the average velocity of the water. This observation can be explained by considering the role of the porous medium. The pressure difference in the wetting phase along a ganglion with projected length L_g, is of order $O(V_f \mu_w L_g/k)$. Notice that for linear ganglia the reduced ganglion length, L_g/l, is roughly equal to the reduced ganglion volume. The pressure drop inside the ganglion is of the order $O(\epsilon \bar{u}_z m_w L_g/k)$. Neglecting the effect of the capillary pressure, the two pressure differences are equal, from which it

follows that $u^* = \epsilon \bar{u}_z / V_f = O(\mu_w/\mu_o) = O(1/\kappa)$, or $\kappa u^* = O(1)$. This argument is valid when Ca is substantially larger than Ca_{cr}, so that capillary effects are negligible. Closer to the critical Ca value, the capillary pressure cannot be neglected. Taking capillarity into account we get

$$\kappa u^* = O(1) - O(k\sigma_{ow}\Delta J / V_f \mu_w L_g),$$

where ΔJ is a measure of the difference in curvature between the meniscus at the nose of the ganglion and the meniscus at the tail of the ganglion. When $O(k\sigma_{ow}\Delta J / V_f \mu_w L_g \ll 1)$, this estimate reduces to $\kappa u^* = O(1)$.

- For fixed values of the reduced ganglion volume, v^*, the reduced time-averaged ganglion velocity, u^*, increases with Ca. In the range of Ca values studied and for $\kappa \leqslant 1$, u^* seems to tend to an asymptotic value, which depends on κ but not on Ca. For $\kappa > 1$, an asymptotic value was never reached in the range of Ca values covered in this study (up to 10^{-2}).
- For fixed values of Ca that are slightly higher than Ca_{cr}, u^* increases monotonically with v^*, reaching an asymptotic value for v^* circa 12 to 15. The asymptotic value depends on κ.
- For $\kappa \geqslant 1$ and fixed Ca, u^* tends asymptotically to a constant value (which depends on the value of Ca) as v^* becomes large (say $v^* > 10$). The behaviour of u^* for small v^* depends on Ca. For relatively small Ca values, u^* becomes nil (the ganglion gets stranded) for some value of v^* that depends on Ca. For large Ca values, u^* increases as v^* decreases and reaches high values at $v^* = 2$.
- For $\kappa < 1$ and fixed Ca, u^* tends asymptotically to a constant value (which depends on the value of Ca) as v^* becomes large (say $v^* > 15$). The value of u^* decreases monotonically as v^* decreases; if Ca is sufficiently small, then u^* becomes nil at some value of v^* that depends on Ca.

Figures 16 and 17 show the effects of an intermediate wettability on ganglion velocity. The viscosity ratio is set at $\kappa = 7$, and the contact angles are taken as $\theta_e = \theta_a^o = \theta_r^o = 10°$ in figure 16 and as $\theta_e = \theta_a^o = \theta_r^o = 30°$ in figure 17. Comparing these results with those of figure 13 the following conclusions can be drawn:

- The critical value for mobilization decreases as θ_e increases. This, of course, is expected.
- For large values of Ca (say $Ca = 5 \times 10^{-3}$), the reduced ganglion velocity decreases as θ_e increases. This could be due to the fact that for fixed v^* the length of a ganglion decreases as θ increases. Shorter ganglia experience a smaller driving force (i.e. pressure difference from tail to nose).
- As seen above, when $\kappa > 1$, Ca = const. and $\theta_e = \theta_a^o = \theta_r^o = 0°$, the value of u^* for small ganglia ($v^* = 2$ or 3) is higher than that for large ganglia. This difference increases as θ increases. The reason for this could be the decrease of capillary resistance to the flow caused by the reduction in the curvature of the menisci. This decrease is more important in the case of small ganglia, since for large ganglia the viscous resistance is dominant.

Figure 18 shows the effect of the contact-angle hysteresis and of the rate-dependency of the contact angles. The viscosity ratio is set as the same value as the previous two figures, $\kappa = 7$, and the limiting contact angles are taken as $\theta_e = 10°$, $\theta_a^o = 11.4°$ and $\theta_r^o = 0°$. Here we assume that the advancing contact angle is rate-dependent as represented by curve c of figure 19. Comparing the results of figure 18 to those of figure 16 we see that contact-angle hysteresis and rate-dependency do not affect substantially the values of u^* for large ganglia and/or large Ca values. However, it

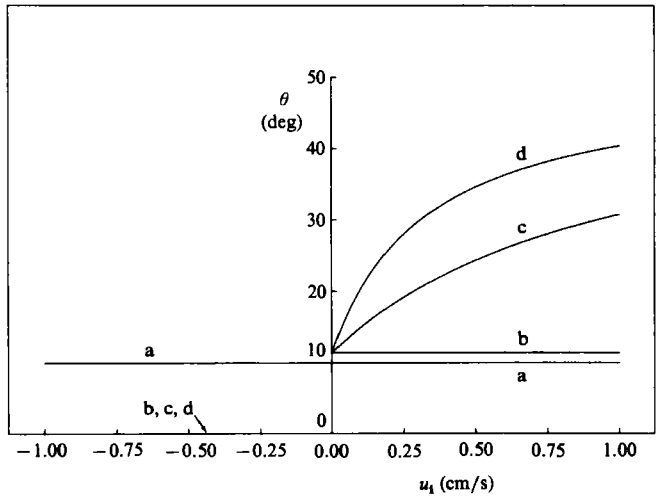

FIGURE 19. Plot of the dependence of the dynamic contact angle, θ, on the interfacial velocity, u_t, for $\theta_e = 10°$, $\theta_a^0 = 11.4°$, $\theta_r^0 = 0°$. Class II hysteresis.

should be noted that the critical capillary numbers and the velocities of small ganglia may be affected significantly when contact-angle hysteresis and rate-dependency are substantial.

6. Conclusions

The motion of oil ganglia in porous media is modelled in the present work by using a network of unit cells of the constricted-tube type, together with an electrical analogue analysis (to calculate the pressure at the nodes and the flowrates in the unit cells) and a set of rules concerning the behaviour of menisci at the nodes. This simulation method is an extension and improvement of the method developed by Payatakes *et al.* (1980) and Ng & Payatakes (1980); it takes into account the viscosities of both fluids; time appears explicitly and flowrates and ganglion velocities are calculated readily; motion of two or more downstream menisci simultaneously, which is an important feature of dynamic displacement, is allowed. The earlier method had the advantage of producing results with relatively small computational effort, and it has been proven to give good results under conditions of quasi-static displacement, but it did not consider rates and it did not apply to dynamic displacement.

The main conclusions that can be drawn from the study of the motion of solitary oil ganglia are the following:

- The parameters that affect the fate of solitary oil ganglia are the capillary number, Ca, the viscosity ratio, κ, the advancing and receding contact angles (θ_a and θ_r, respectively), the ganglion size (expressed in terms of the reduced ganglion volume, v^*), the local geometry of the porous medium, and the orientation of the macroscopic pressure gradient relative to the network.
- Two different types of displacement are observed, depending on the value of the capillary number. If the capillary number is close to the critical value for mobilization for a given ganglion, Ca_{cr}, the ganglion moves with only one downstream meniscus at any time (quasi-static displacement). In this case it tends to become elongated and aligned with the direction of flow. While it

moves it frequently breaks into daughter ganglia, the smaller ones of which quickly get stranded. Break-up is due mostly to pinch-off. Restranding of a mobilized ganglion can occur even without break-up. If the capillary number substantially exceeds Ca_{cr}, the ganglion undergoes dynamic displacement, that is, it may advance with two or more downstream menisci simultaneously. The tendency for elongation is much smaller than in the case of quasi-static displacement, and the rate of break-up per unit length of travel is much higher. Break-up is mainly due to the mechanism of dynamic break-up, even though pinch-off is still significant.

- The rates of break-up and stranding were studied with the simulator and the results are expressed in terms of the break-up and stranding coefficients and of the break-up mode probability. It is found that the stranding coefficient decreased with increasing capillary number. In contrast, the break-up coefficient increases as Ca increases. The viscosity ratio seems to affect the break-up coefficient only weakly. For small Ca values the dominant mechanism of break-up is pinch-off and the daughter ganglia are usually quite unequal. For large Ca values the dominant mechanism is dynamic break-up and the daughter ganglia are usually of comparable size. Pinch-off is significant, however, even at high Ca values.
- The ganglion velocity can be expressed in terms of the reduced time-averaged ganglion velocity, u^*. This velocity is smaller than unity if the viscosity ratio is unfavourable ($\kappa \geqslant 1$), and larger than unity if the viscosity ratio is favourable ($\kappa < 1$) and the ganglion is large. In general, u^* increases with increasing Ca. For ganglia larger than about 5 chambers, u^* increases with increasing ganglion size, and for very large ganglia it may reach an asymptotic value that depends on Ca and κ. The behaviour of smaller ganglia is more complex. If the value of Ca is close to the critical value for mobilization, Ca_{cr}, u^* increases monotonically with v^*. For values of Ca that are substantially higher than Ca_{cr}, the velocity of 2- and 3-chamber ganglia may be slightly larger than the velocity of larger ganglia. This effect is observed in the simulations of this work only for $\kappa \geqslant 1$. u^* is also found to depend on the contact angle and to a lesser degree on contact-angle hysteresis. As the equilibrium contact angle increases, the critical capillary number for mobilization decreases. For Ca substantially larger than Ca_{cr}, u^* decreases as θ_e increases.

Most of this work was done at the University of Houston, with support from US Department of Energy, Grant No. E(40-1)-5075, and a grant from Schlumberger–Doll Research. Some simulations were performed at SDR Center.

REFERENCES

BATYCKY & SINGHALL 1977 Mobilization of entrapped ganglia. *Res. Rep.* RR-35, Petroleum Recovery Institute, Calgary, Canada.

DIAS, M. M. 1984 Formation and dynamics of oil ganglia in porous media. Ph.D. dissertation, University of Houston, Houston, Texas.

DIAS, M. M. & PAYATAKES, A. C. 1986 Network models for two-phase flow in porous media. Part 1: Immiscible microdisplacement of non-wetting fluids. *J. Fluid Mech.* **164**, 305–336.

EGBOGAH, E. O. & DAWE, A. 1981 A model of oil ganglion movement in porous media. SPE 10115, *56th Annual Fall Tech. Conf. and Exhib. of SPE*, San Antonio, Texas, Oct. 5–7.

HINKLEY, R. E. 1982 Oil ganglion motion. M.S. thesis, University of Houston, Houston, Texas.

HINKLEY, R. E., DIAS, M. M. & PAYATAKES, A. C. 1985 On the motion of oil ganglia in porous media. To appear.

LEGAIT, B. 1981 Influence des forces d'inertie et de viscosité sur la difference de pression nécessaire au passage d'une goutte, immiscible avec le fluid en place, à traverse un col. *C.R. Acad. Sci. Paris*, **292**, Sér II, 1111–1114.

LEGAIT, B. & JACQUIN, C. 1982 Conditions nécessaires au passage d'un col par une goutte en déplacement dans un capillaire de section carrée, en régime de Stokes. *C.R. Acad. Sci. Paris*, **294**, Sér. II, 487–492.

LEVERETT, M. C. 1941 Capillary behavior in porous solids. *AIME Trans.* **142**, 152–169.

MELROSE, J. C. & BRANDNER, C. F. 1974 Role of capillary forces in determining microscopic displacement efficiency for oil recovery by water flooding. *J. Can. Pet. Tech.* **13** (4), 54–62.

NG, K. M. 1980 Oil ganglia dynamics in flow through porous media. Ph.D. thesis, University of Houston, Houston, Texas.

NG, K. M., DAVIS, H. T. & SCRIVEN, L. E. 1978 Visualization of blob mechanisms in flow through porous media. *Chem. Eng. Sci.* **33**, 1009–1017.

NG, K. M. & PAYATAKES, A. C. 1980 Stochastic simulation of the motion, break-up and stranding of oil ganglia in water-wet granular porous media during immiscible displacement. *AIChE J.* **26**, 419–429.

OH, S. G. & SLATTERY, J. C. 1979 Interfacial tension required for significant displacement of oil. *Soc. Pet. Eng. J.* **19**, 83–96.

OLBRICHT, W. L. & LEAL, L. G. 1983 The creeping motion of immiscible drops through converging/diverging tubes. *J. Fluid Mech.* **134**, 329–355.

PAYATAKES, A. C. 1982 Dynamics of oil ganglion during immiscible displacement in water-wet porous media. *Ann. Rev. Fluid Mech.* **14**, 365–393.

PAYATAKES, A. C. & DIAS, M. M. 1984 Immiscible microdisplacement and ganglion dynamics in porous media. *Rev. Chem. Eng.* **2** (2), 85–174.

PAYATATAKES, A. C., NG, K. M. & FUMERFELT, R. W. 1980 Oil ganglia dynamics during immiscible displacement. Model formulation. *AIChE J.* **20**, 430–443.

PAYATAKES, A. C., TIEN, CHI & TURIAN, R. M. 1973 A new model for granular porous media – Part I. Model formulation. *AIChE J.* **19**, 67–76.

PAYATAKES, A. C., WOODHAM, G. & NG, K. M. 1981 On the fate of oil ganglia during immiscible displacement in water wet granular porous media. In *Surface Phenomena in Enhanced Oil Recovery* (ed. D. O. Shah). Plenum Press, New York.

RAPIN, S. 1980 Behavior of non-wetting oil ganglia displaced by an equeous phase. M.S. thesis, University of Houston, Houston, Texas.

YADAV, G. D. & MASON, G. 1983 The onset of blob motion in a random sphere packing caused by flow of the surrounding liquid. *Chem. Eng. Sci.* **38**, 1461–1465.